

Interpretation of the deep cracking phenomenon of tungsten monoblock targets observed in high-heat-flux fatigue tests at 20 MW/m²

Muyuan Li, Jeong-Ha You*

Max-Planck-Institut für Plasmaphysik, Boltzmannstr.2, 85748 Garching, Germany

Highlights

- A theoretical interpretation is presented for the observed deep cracking feature observed in the high heat flux tests of tungsten monoblocks at 20 MW/m².
- A two-stage modelling approach is employed where deep cracking is thought to be a consecutive process of crack initiation and crack growth.
- The fatigue lifetime to crack initiation on the armor surface and the crack tip load of brittle fracture are assessed.
- Numerical predictions in this study agree well with the experimental observed findings.

Abstract

The HHF qualification tests conducted on the ITER divertor target prototypes showed that the tungsten monoblock armor suffered from deep cracking due to fatigue, when the applied high-heat-flux load approaches 20 MW/m². In spite of the critical implication of the deep cracking of armor on the structural integrity of a whole target component, no rigorous interpretation has been given to date. In this paper, a theoretical interpretation of the observed deep cracking feature is presented. A two-stage modelling approach is employed where deep cracking is thought to be a consecutive process of crack initiation and crack growth, which is assumed to be caused by plastic fatigue and brittle fracture, respectively. The fatigue lifetime to crack initiation on the armor surface and the crack tip load of brittle fracture are assessed as a function of crack length and heat flux loads. The potential mechanisms of deep cracking are discussed for a typical slow transient high-heat-flux load cycle. It is shown that the quantitative predictions delivered in this study agree well with the observed findings offering insight into the nature of tungsten armor failure.

Keywords: divertor target, tungsten armor, high heat flux loads, fracture mechanics, crack, plastic fatigue

1. Introduction

Maintenance of structural integrity under high-heat-flux (HHF) fatigue loads is a critical concern for assuring the reliable HHF performance of a plasma-facing divertor target component. Loss of structural integrity may lead to structural as well as functional failure of the component. Such failure is difficult to predict theoretically, unless material parameters and constitutive laws of damage (and cracking) are well defined. Thus, the structural integrity of a target is evaluated primarily on an empirical basis by means of HHF fatigue tests. For sensible interpretation of the experimental findings, however, rigorous theoretical scrutiny is still desired.

Recently, a series of HHF fatigue test campaigns have been conducted for the qualification of tungsten monoblock target technology developed for the full-tungsten divertor of ITER [1, 2]. The design specification of HHF fatigue defined for the ITER tungsten target is as follows:

5000 cycles at 10 MW/m^2 (stationary thermal load)

300 cycles at 20 MW/m^2 (slow transient thermal load)

The results of the HHF fatigue tests, which were obtained using small- or medium scale mock-ups, showed that the specification of HHF fatigue life could be a demanding requirement in the case of the slow transient thermal load (20 MW/m^2) whereas the stationary load (10 MW/m^2) indicated no serious challenge in terms of fatigue performance [3, 4]. Hence, we will focus our discussion on the HHF fatigue at 20 MW/m^2 only in what follows.

The previous post-mortem investigation of the tested mock-ups showed that the tungsten armor blocks experienced fatigue cracking at 20 MW/m^2 [3]. The cracks were initiated at the armor surface and grew toward the cooling tube in the vertical direction (see Fig. 1). Initially several small cracks were formed on the surface, but a single crack grew further as major crack reaching a macroscopic length. After several hundreds of HHF load cycles at 20 MW/m^2 , the major crack almost reached the copper interlayer adjacent to the tube. The site of major cracks was located at the mid-region of the monoblock.

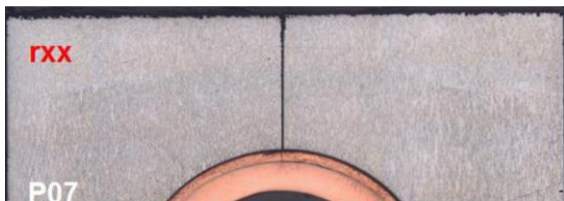


Fig. 1. Metallographic cross section of a prototypical ITER divertor target component after HHF test at 20 MW/m² (300 HHF load cycles) [3].

Metallographic analyses of the tungsten block cross sections revealed that the upper part of the armor block underwent an apparent microstructural change during the HHF loading at 20 MW/m². Roughly, one-third part of the armor block from the top surface turned out to be recrystallized due to severe thermal exposure. The near-surface region exhibited a characteristic pattern of plastic grain deformation while the feature of crack growth indicated a brittle failure. From this finding, it was speculated by the test team that the cracks on the tungsten surface had been initiated as a result of plastic low cycle fatigue (LCF). A possible scenario of cracking mechanism by LCF and thermal stress could be reconstructed as follows:

1. The surface of armor block is excessively heated up under the HHF load of 20 MW/m². The temperature of the surface rises so strongly that the surface layer of tungsten armor loses most of its yield strength due to thermal softening [5].
2. During heating plastic yield occurs in the near-surface region due to thermal stress.
3. Upon by the brittleness of tungsten. Ductile-to-brittle transition (DBT) of tungsten during cooling promotes the cracking. Cracking is more critical for the recrystallized tungsten.

Now, the question is whether this scenario is physically possible or not. The aim of this paper is to answer this question by delivering the quantitative assessments of the plastic fatigue lifetime of tungsten armor surface and the driving force of cracking in the tungsten armor block. To this end, a full HHF load cycle is simulated by means of coupled thermal and (fracture-) mechanical 3D finite element analyses (FEA). As reference FEA model, one of the standard ITER target mock-ups is used for direct comparison with the previous experimental results. For comparative study, the assessment is made for a range of HHF loads between 10 and 20 MW/m².

In the first part of the study, the fatigue lifetime of armor surface is estimated to judge whether a fatigue crack can be formed by LCF within the range of tested HHF load cycles. In the second part, the crack tip load is computed and compared with the fracture toughness to judge whether a major crack can further grow reproducing the observed fracture pattern.

2. Model for finite element analysis

2.1. Geometry, FEA mesh and materials

The geometry of the present FEA model was adopted from the ITER divertor target design. The target component is a duplex structure consisting of tungsten monoblock as armor and CuCrZr alloy cooling tube as heat sink. A symmetric quarter part model (half width and half depth) was used as illustrated in Fig. 2. for the sake of brevity. The dimension of the test mock-ups used for the HHF tests in [4] was considered for the current modelling. The single tungsten block has the dimension of $28 \times 28 \times 12 \text{ mm}^3$. The cooling tube has a thickness of 1.5 mm and an inner diameter of 12 mm, while the thickness of the copper interlayer is 1 mm. The shortest distance from the armor surface to the interlayer is 6.5 mm. Commercial FEA code ABAQUS was employed. The 3D model consisted of roughly 19000 quadratic brick elements.

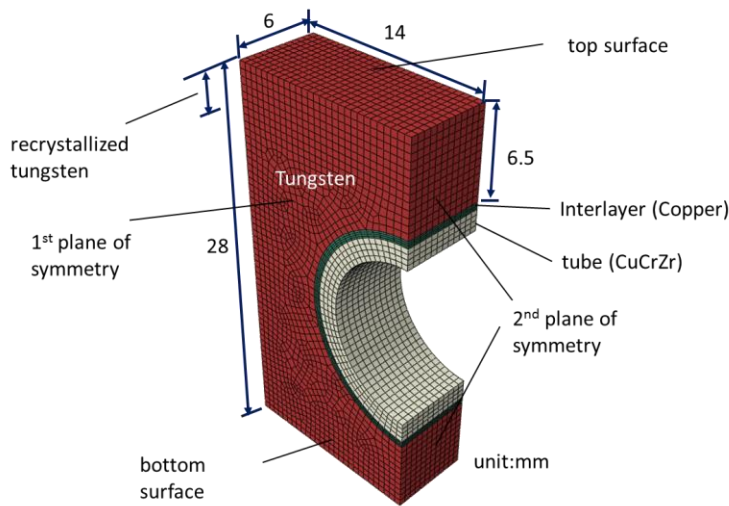


Fig. 2. Geometry and mesh of the FEA model (symmetric quarter part model).

Tungsten was assumed to be linear elastic and ideal-plastic whereas kinematic hardening was not taken into account due to the lack of material data. This assumption can be justified by the fact that the surface experiences extremely high temperature losing the memory of internal state variables (e.g. hardening variables) during each HHF loading. As the upper part of the tungsten block was assumed to be recrystallized, two different sets of plastic material data were used for the tungsten armor: recrystallized grade for the upper part and stress-relieved grade for the lower part. The thickness of the recrystallized layer was varied from 0 to 4 mm.

Precipitation-hardened CuCrZr alloy was considered for the heat sink tube. Soft copper was assumed for the interlayer. The combined non-linear isotropic and kinematic hardening law was applied for the copper and copper alloy where Frederick-Armstrong type kinematic hardening constitutive law was assumed [7-9]. Selected material parameters are listed in Table 1.

Table. 1. Properties of the considered materials at selected temperatures [10-12].

	Tungsten ¹ (recrystallized ²)				CuCrZr ³		Copper ⁴		
	20°C	400°C	1200°C	2000°C	20°C	400°C	20°C	400°C	
Young's modulus (GPa)	398	393	256	285	115	106	115	95	
Yield stress (MPa)	1384 (377)	947 (362)	346 (223)	57 (70)	373	319	56	31	
Heat conductivity (W/mK)	173	140	105	99	318	347	379	352	
Coefficient of thermal expansion (10 ⁻⁶ /K)	4.5	4.63	4.98	5.43	16.7	18.1	16.7	18.2	
Material parameters entering the Frederick-Armstrong constitutive model for CuCrZr and copper.					σ^0 (MPa)	273	238	3	3
					Q (MPa)	-43	-68	76	36
					b	6	10	8	25
					C(MPa)	148575	117500	64257	31461
					γ	930	1023	888	952

¹ Rolled and stress-relieved state.

² The ultimate tensile strength of recrystallized tungsten is used as yield stress assuming a pre-hardened state.

³ Precipitation-hardened state, the reference alloy: Elmedur-X (code: CuCr1Zr, Cr: 0.8%, Zr: 0.08%).

⁴ Softened by annealing at 700°C for 1 h.

2.2. Loads and boundary conditions

The full thermal history of a typical target mock-up was considered for modelling. The thermal history includes fabrication, stand-by, HHF loading and cooling stages as illustrated in Fig. 3. The effective stress-free temperature is set equal to the final heat treatment temperature (450 °C) of the joined mock-up where prime ageing of the precipitates in the microstructure of CuCrZr alloy should takes place leading to precipitation hardening. It is assumed that the previous residual stress disappears during annealing, and the final residual stress is solely dictated by the thermal strain mismatch during cooling from 450 °C to room temperature. The thermal history consists of four steps as follows:

1st step: cooling from the stress-free temperature to room temperature.

2nd step: pre-heating to the stand-by temperature.

3rd step: HHF loading.

4th step: cooling to the coolant temperature.

The main applied heat flux load was 20 MW/m², but 10 and 15 MW/m² were also considered for comparison.

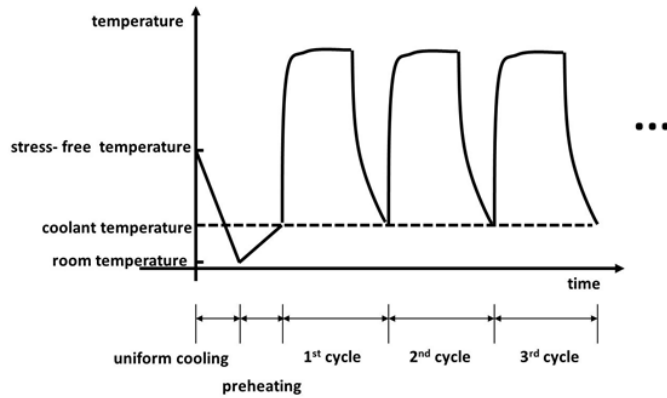


Fig. 3. Schematic illustration of the thermal history considered for modelling.

The real cooling condition was assumed that was actually applied for the HHF test. The cooling parameters are as follows.

- pressure: 3.3 MPa
- temperature: 120 °C
- velocity: 12 m/s.

The selected values of heat transfer coefficient calculated using Sieder/Tate [13] and CEA/Thom [14] correlations (with swirl tape) are listed in Table 2. The local critical heat flux at the tube is estimated to be 38 MW/m² using the modified Tong 75 correlation formulated by CEA [14]. In the current thermal simulation, this critical heat flux value was not reached by the given HHF loads.

Table. 2. Selected values of heat transfer coefficient calculated for the current cooling condition.

	100 °C	150 °C	200 °C	250 °C	295 °C
heat transfer coefficient (kW/m ² ·K)	109.1	115.92	121.01	128.75	208.24

In the stress analysis, kinematic constraint was applied to the end sections of the tube to suppress

the axial displacement. As the fracture-mechanical analysis made in this study was deterministic in nature, two most potential cracking sites were predefined and the crack tip load was computed in an incremental manner for increasing crack length.

3. Results and discussion

3.1. Thermal response

Fig. 4 shows the calculated temperature field in the divertor target under stationary HHF load of 20 MW/m². Steep temperature gradient is built in the upper part of the tungsten block, which is a characteristic feature of the HHF loading of water-cooled targets. In Table 3, the temperature ranges on the armor surface during steady state loading are summarized for three different HHF loads. It is seen that the armor surface is heated up well above the recrystallization temperature of tungsten (roughly 1300 °C [15]) under both 15 and 20 MW/m² while the peak temperature under 10 MW/m² is far below 1300 °C.

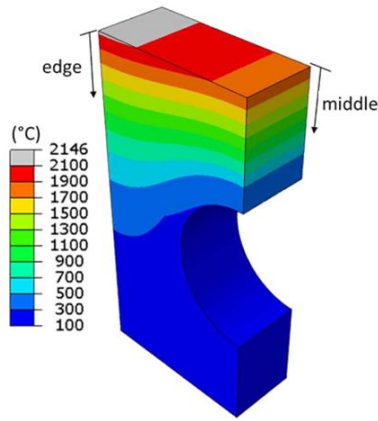


Fig. 4. Temperature field in the divertor target under stationary HHF load of 20 MW/m².

Table. 3. Calculated temperature range on the armor surface during steady state HHF loading.

Heat flux loads	Temperature ranges
10 MW/m ²	950-1058 °C
15 MW/m ²	1411-1612 °C
20 MW/m ²	1864-2146 °C

After a large number of HHF load cycles, the total duration of the repeated thermal loading at power density higher than 15 MW/m² may provide the material enough time to recrystallize in

the upper part of the armor block where the local temperature becomes higher than 1300 °C. Indeed, it has been experimentally found that a substantial part of a tungsten armor block can be recrystallized starting from the top surface after hundreds of HHF load pulses at power density above 15 MW/m² (the higher the power density, the larger the recrystallized depth) [3].

So, in this study, the recrystallized depth was defined as the distance from the top surface to the average vertical position in the tungsten block where the local temperature was 1300 °C. Here, 1300 °C was assumed as the threshold temperature for recrystallization considering sufficiently long cumulative thermal exposure.

The results are given in Table 4. Obviously, the estimated depth is quite different between the edge and middle positions. This result fits well to the experimental observation [3].

The temperature field in the target, thus the recrystallized depth, sensitively depends on the thickness of tungsten armor between the surface and the tube. For instance, when the armor thickness is reduced to 5 mm, then recrystallization would not take place under 15 MW/m² (max. temperature reaches only 1220 °C) [16].

For simplicity, in the simulations a 4 mm recrystallized layer was assumed for 20 MW/m² and a 2 mm recrystallized layer for 15 MW/m². No recrystallized layer is assumed for 10 MW/m².

Table. 4. Estimated depth of recrystallized part in the tungsten armor block. Sufficiently long time of cumulative thermal exposure was assumed.

	Edge line	Middle axis
10 MW/m ²	0 mm	0 mm
15 MW/m ²	2 mm	0.5
20 MW/m ²	4.5 mm	2.5 mm

3.2. Crack initiation by low cycle fatigue

When tungsten is recrystallized, the yield stress decreases significantly as indicated in Table 1. For the same applied stress, recrystallized tungsten undergoes much larger plastic deformation than cold-rolled or stress-relieved one, provided the loading temperature is higher than the DBT temperature. Thus, recrystallized tungsten has higher risk to suffer from plastic LCF than the cold-worked one, since larger amount of plastic strains will be produced and accumulated due to low yield stress.

Fig. 5 shows the plastic strain field in the tungsten armor block after the 5th HHF load cycle at 20 MW/m². Plotted is the accumulated equivalent plastic strain which is a scalar-valued measure of plastic work incurred in a multi-axial strain state. It is found that the accumulated plastic strain is concentrated exclusively in the near-surface region of the tungsten armor while the rest part of the block remains only elastic. The strongest concentration appears in the middle region of the armor surface, where the maximum value amounts to 0.036 (3.6 %) after the 5th HHF load cycle.

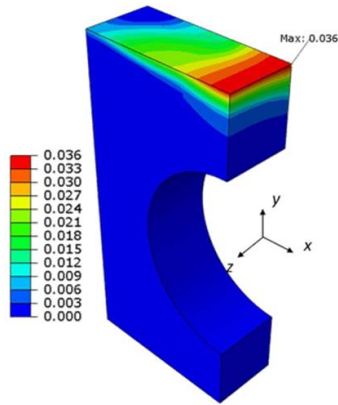


Fig. 5. Accumulated equivalent plastic strain field in the tungsten armor block after the 5th HHF load cycle at 20 MW/m². Only the tungsten armor block is shown.

Plastic LCF failure is dictated by the magnitude of strain amplitudes, which is indicated by the increment of accumulated equivalent plastic strains during stabilized cyclic loading.

Fig. 6 shows the evolution of accumulated equivalent plastic strain at the location of peak plastic strain (i.e. the middle position on the armor surface). The plastic strains are plotted over the first five HHF load cycles for two different HHF loads (i.e. 15 and 20 MW/m²). The loading at 10 MW/m² produced no plastic strain. The strain increments seem to be saturated after 5 HHF load cycles in all cases. The graph shows that the tungsten surface experiences much severer plastic deformation and larger plastic strain increments under 20 MW/m² than 15 MW/m². It is also found that the low yield stress due to recrystallization has a significant impact on the plastic straining of the tungsten armor surface. The total accumulated plastic strain of the recrystallized surface layer is four times larger than that of stress-relieved tungsten armor.

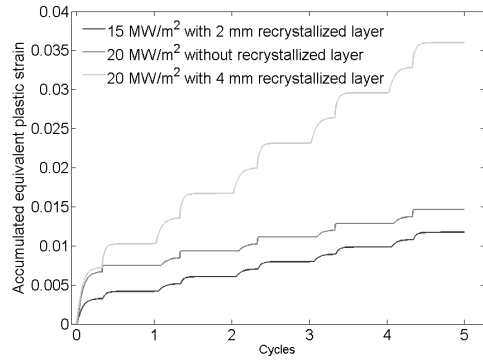


Fig. 6. Accumulated equivalent plastic strain at the reference node as a function of time for different HHF loads.

Now, LCF lifetime can be assessed using the computed strain increment and experimental LCF data. Little data is available on the LCF behavior of tungsten. In Fig. 7, the LCF curves of two different tungsten grades (stress-relieved and annealed) are plotted where the data were fitted to the Manson-Coffin relation [12]. The LCF lifetime of stress-relieved tungsten is much greater at 815 °C than that at room temperature. This may be attributed to the brittleness of tungsten at RT (DBT temperature lies around 600-800 °C). It is also seen that annealed (recrystallized) tungsten has higher LCF lifetime than stress-relieved one at 815 °C above 10⁴ cycles.

Fatigue life is usually estimated by substituting the amplitude of plastic strain in uniaxial stress state (half of the increment of accumulated equivalent plastic strain in multi-axial strain states) into the empirical Manson-Coffin equation obtained for given test temperature. In the context of present study, the LCF life should be interpreted as the number of cycles to crack initiation.

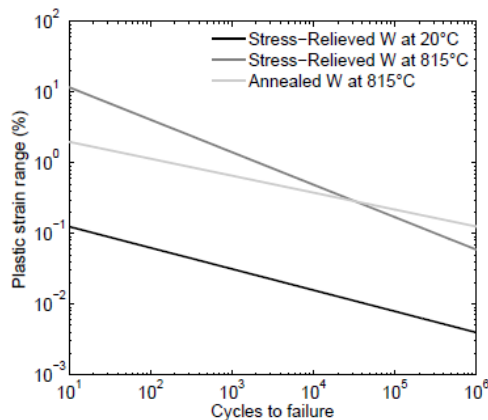


Fig. 7. Experimental LCF data of two different tungsten grades (stress-relieved and annealed) fitted by the Manson Coffin relation [12].

The loading temperature is assumed to be same as the test temperature at which the LCF life data are measured. In the present study, however, the situation is different: the evolution of plastic strain takes place during transient temperature development. Thus, it is by no means a trivial question how to compare the computed strain amplitude with a specific LCF data measured by isothermal test condition.

This issue is clearly illustrated in Fig. 8 where the temperature fluctuation and the evolution of accumulated equivalent plastic strain are plotted together over the common time scale of a HHF pulse at 20 MW/m² (5th HHF load cycle, at the reference position).

It is found that the plastic strain is produced only during the transient stages of the thermal cycle, both in heating and cooling phases. Considering that the DBT temperature substantially affects the ductility, and thus the LCF behavior of a metal, we divided the total plastic strain amplitude into two components, namely, strain increment being produced above and below 800 °C, respectively. The contribution of each part to the final LCF life can be taken into account by means of Miner's rule, which writes:

$$\frac{1}{N} = \frac{1}{N_{low}} + \frac{1}{N_{high}} \quad (1)$$

where N_{low} and N_{high} are the numbers of cycles to failure due to the plastic strain amplitude each produced below 800°C ($\Delta\varepsilon_p^{800-}$) and above ($\Delta\varepsilon_p^{800+}$) 800 °C, respectively. The contribution of each strain increment to the LCF lifetime is then estimated by using different LCF data obtained at approximately similar test temperatures.

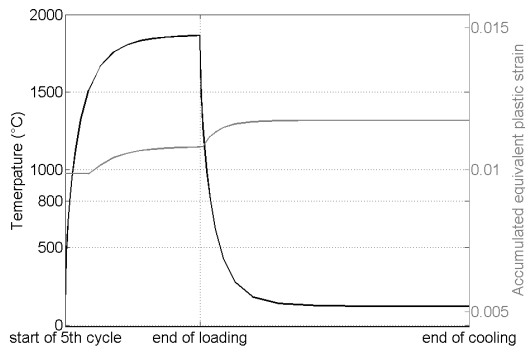


Fig. 8. Evolution of surface temperature and the maximum accumulated equivalent plastic strain over the common time scale of HHF pulse at 20 MW/m² (5th HHF load cycle).

Table 5 shows the predicted minimum LCF lifetime of the tungsten armor surface together with the estimated equivalent plastic strain range (%). If there is a 4 mm thick recrystallized layer below the surface, roughly 20 % of the total plastic strain is predicted to be produced below 800 °C under the HHF load of 20 MW/m² while the rest is produced above 800 °C. If there is no recrystallization, plastic strain is produced only above 800 °C.

Table 5. Equivalent plastic strain range (%), $\Delta\varepsilon_p$ and the predicted LCF lifetime (number of cycles to crack initiation) assessed for the tungsten armor surface.

	20 MW/m ² with 4 mm recrystallized layer	20 MW/m ² without recrystallized layer	15 MW/m ² with 2 mm recrystallized layer
$\Delta\varepsilon_p^{800-}$	0.065	0	0.036
$\Delta\varepsilon_p^{800+}$	0.260	0.087	0.058
N_{low}^1	87	No failure	618
N_{high}^2	4.8×10^4	4.5×10^6	2.5×10^6
N_{high}^3	4.0×10^4	4.2×10^5	1.0×10^6
N	86	4.2×10^5	617

¹ estimating with the plastic strain range generated below 800°C based on LCF data of stress-relieved tungsten at 20°C.

² estimating with the plastic strain range generated above 800°C based on LCF data of annealed tungsten at 815°C.

³ estimating with the plastic strain range generated above 800°C based on LCF data of stress-relieved tungsten at 815°C.

The results of the LCF estimation can be summarized as follows:

1. The tungsten armor ‘without’ recrystallized layer would experience no cracking by LCF even at 20 MW/m² owing to its high yield stress (thus small plastic strain).
2. The tungsten armor ‘with’ recrystallized layer is subjected to cracking by LCF under HHF loads of 15-20 MW/m² owing to its low yield stress (thus large plastic strain).
3. The main cause of cracking by LCF is the plastic strain increment during cooling at lower temperatures below the DBT temperature where tungsten becomes brittle. This

means that the cooling stage alone determines the cracking behavior.

4. The number of load cycles to cracking estimated for the recrystallized tungsten armor surface is 86 for 20 MW/m² and 617 for 15 MW/m².

The large residual stress generated by the plastic yield during HHF loading can possibly trigger the brittle cracking of tungsten armor as well [17].

3.3. Crack growth by thermal stress

In the previous section it was shown that cracks can be initiated on the tungsten armor surface as a result of LCF damage. In this section, attention is shifted from initiation to the growth of a created crack during a HHF load cycle. Two conditions have to be met for a crack to grow in the presence of thermal stress fields: first, a crack is loaded by tensile stress in crack opening mode (tearing or sliding mode is not possible to occur in a single material) and second, the crack tip load is greater than the material's resistance against crack extension. The second criterion can be expressed in terms of either stress intensity factor vs. fracture toughness or strain energy release rate vs. fracture energy. A scalar-valued quantity, J -integral, is a measure of strain energy release rate of a crack in nonlinear elastic (or brittle plastic) materials. In the followings, the two conditions are examined for the given HHF loading cases in a quantitative way.

Fig. 9 shows the thermal stress fields (Cartesian normal component in the x direction) produced in the tungsten armor block at 5th HHF load cycle at 20 MW/m². Plotted are the stress states in the stationary thermal loading stage and in the stationary cooling phase, respectively. It is seen that the tensile stress regions are situated at different locations: during HHF heating tensile stress appears in the vicinity of the tube whereas it occurs near the surface during cooling. Such strong tensile stress can cause crack initiation even without LCF damage, if there is a microscopic flaw where applied stress is concentrated. Hence, crack initiation at both locations of the tensile stress regions is regarded highly probable. In this sense, the two crack positions were considered for the fracture mechanics study here, as illustrated in Fig. 10. J -integral around the assumed crack tips was calculated to assess the driving force of crack growth. The criterion for crack growth is met when the J -integral value exceeds the critical fracture energy for the given temperature.

The tensile stress fields indicate that the initiated cracks will extend in vertical direction. The length of the pre-cracks was assumed to be 0.5 mm long.

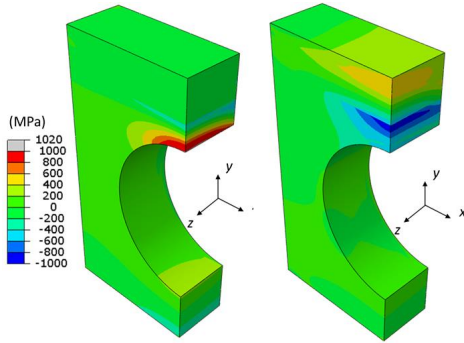


Fig. 9. Thermal stress fields (normal component x direction) in the tungsten armor block at 5th HHF load cycle at 20 MW/m² during heating (left) and during cooling (right). The tube and the interlayer are not shown.

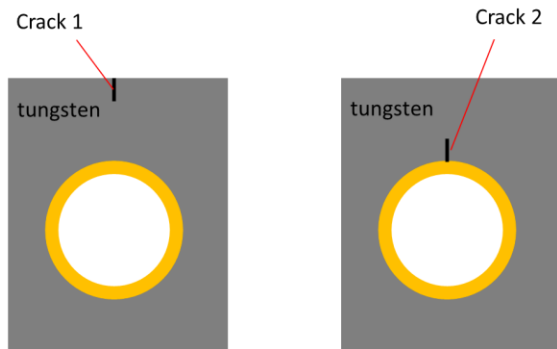


Fig. 10. Locations of crack considered for the fracture mechanics analysis. The length of the pre-cracks was assumed to be 0.5 mm long.

Fig. 11 presents the J -integral values at 20 MW/m² calculated for the surface crack (crack 1) as a function of crack length. Two different sets of J -integral values are presented, each calculated either at the free surface edge or at the 1st symmetry plane (see Fig. 1), respectively. For comparison, the literature data [18] of critical fracture energy measured at 400 °C is also plotted as dotted line. The J -integral data are compared between two stages of a HHF load cycle: stationary heating (a) and the end phase of cooling (b). The crack tip loading behavior of the ‘surface crack’ can be summarized as follows:

1. Once a crack is initiated on the armor surface by any cause (particularly, middle region), it definitely grows, because the crack tip load is much higher than the toughness.

2. In the initial stage of cracking, the crack grows during the cooling phase only. The tensile stress developing upon cooling allows the crack to grow downwards up to 4.5 mm deep. The HHF heating stage has no influence on the small crack (< 5.5 mm)
3. If the crack happens to grow more than 5.5 mm deep (e.g. by fatigue crack growth), then it can grow further during HHF heating until it reaches the interlayer. The cooling stage has no influence on the large crack (> 5 mm).
4. Crack tip is loaded more strongly at the 1st plane of symmetry of the armor than at the free surface. Thus, the crack tip front would be formed into an elliptic contour.

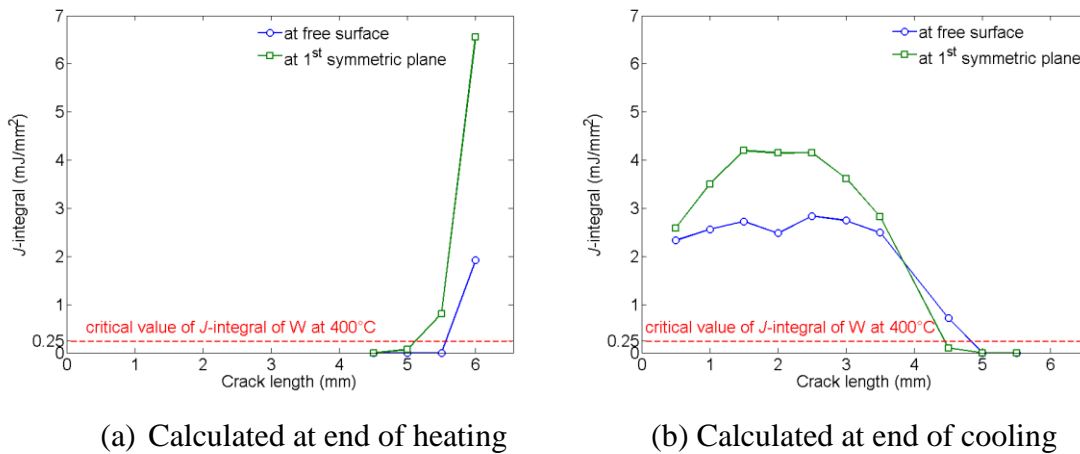


Fig. 11. J -integral values of the surface crack (crack 1) plotted as a function of crack length. The applied HHF load is 20 MW/m^2 . The recrystallized depth is 4 mm. Two different sets of J -integral values are presented, each calculated either at the free surface edge or at 1st plane of symmetry, respectively. For comparison, the fracture energy (critical J -integral) of stress-relieved tungsten at 400°C is plotted (dotted line).

Fig. 12 shows the J -integral values calculated for the crack near the tube (crack 2) as a function of crack length. As the crack experiences only compressive stress during the cooling phase, only the J -integrals during the stationary HHF heating are presented. The trend of fracture behavior can be summarized as follows:

1. Once a crack is created by strong tensile stress in the tungsten block adjacent to the tube, it definitely grows, because the crack tip load is much higher than the toughness.
2. In the initial stage of cracking, the crack grows during the HHF heating phase only. The tensile stress developing upon heating allows the crack to grow upwards up to 2.5-3.5

mm deep. The cooling stage has no influence on the small crack.

3. The crack growth ceases, when the crack length reaches roughly 3.5 mm. The region of tensile stress is situated too far from the crack front to have any influence.

Similar results were already obtained in the previous study of the authors [6].

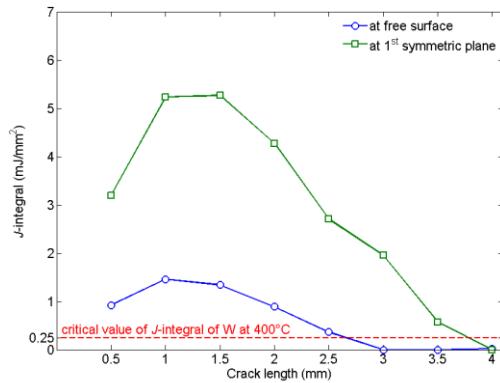


Fig. 12. J -integral values of crack 2 as a function of crack length. The applied HHF load is 20 MW/m². The recrystallized depth is 4 mm. The fracture energy value (critical J -integral) of stress-relieved tungsten at 400 °C is plotted (dotted line) for comparison.

It is noted that the literature data of fracture energy considered in Figs. 11 and 12 were measured for stress-relieved tungsten at 400 °C. Since recrystallized tungsten should have lower fracture energy than this value, the prediction of crack growth behavior discussed above may be rather conservative estimates.

Fig. 13 shows the maximum J -integral values calculated for the two cracks (crack 1 and crack 2) with a length of 1 mm as a function of HHF loads. The cracks were assumed to locate at the 1st plane of symmetry. J -integrals of crack 1 were calculated for the cooling stage, while those of crack 2 for the HHF heating stage.

The trend shows that:

1. The crack initiated on the surface can definitely begin to grow when the applied HHF load is higher than 15 MW/m².
2. The crack initiated near the tube can definitely begin to grow when the applied HHF load is higher than 10 MW/m².

It is reminded that the present conclusions derived from the fracture mechanics analyses assume

the presence of a pre-crack without asking how it has been created. Thus, the correspondence of the predictions made by fracture mechanics analysis with the experimental findings should be evaluated together with the predictions of crack initiation behavior.

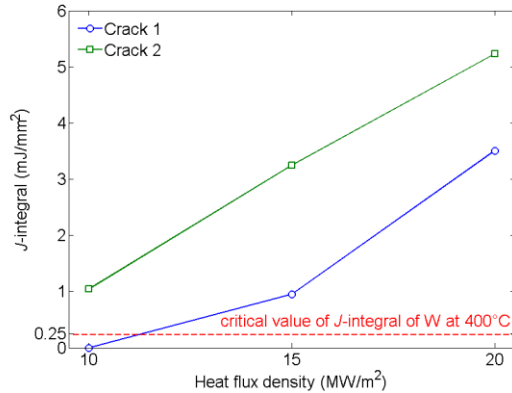


Fig. 13. Maximum J -integral values calculated for the two cracks (crack 1 and crack 2) with a length of 1 mm as a function of HHF loads. The cracks were assumed to locate at the 1st plane of symmetry.

4. Summary and conclusions

The HHF qualification tests conducted on the ITER divertor target prototypes showed that the tungsten monoblock armor suffered from deep cracking due to fatigue as reported in [3], when the applied HHF load approaches 20 MW/m². In this paper, a rigorous theoretical interpretation of the observed cracking features was presented by means of finite element analysis.

Two-track computational approach was employed: 1) to simulate the plastic fatigue of the armor surface for assessing the lifetime to crack initiation and 2) to compute the crack tip load for estimating the driving force of crack growth. The quantitative predictions delivered in this study agreed well with the observed findings offering insight into the mechanisms of deep cracking. Cracks can be initiated on the surface of tungsten armor, if the applied HHF load is about 15 MW/m² or higher under which the tungsten armor begins to be partially recrystallized from the surface layer. The major features predicted by the current study at 20 MW/m² are as follows:

1. Temperature distribution indicates that recrystallization occurs in the upper part of the tungsten armor.
2. The most probably cause of cracking is LCF damage followed by crack formation due to

tensile stress developing in the surface region during cooling stage.

3. LCF damage is promoted by the low yield stress of recrystallized tungsten during HHF heating.
4. Crack initiation is substantially favored in the recrystallized tungsten armor owing to the increased brittleness. Recrystallized tungsten has a much lower LCF life compared to cold-worked tungsten.
5. Once a crack is created on the armor surface, it can grow during the cooling stage where strong tensile stress develops in the upper part of the armor. The crack growth during cooling is predicted to cease at the depth of about 5 mm.
6. Crack growth can be continued during the HHF heating stage where strong tensile stress develops in upper interfacial region of the tungsten armor block adjacent to the top position of the copper interlayer.
7. Crack growth is triggered by strong crack tip opening loads over the whole thickness of the armor except the depth band between 4.5-5.5 mm. Hence, the observed deep cracking should be rather a rule than exception.

Acknowledgement

The authors are grateful to Mr. Alexander von Müller at IPP, Garching for his providing us the data of heat transfer coefficient. This work has been carried out within the framework of the EUROfusion Consortium and has received funding from the Euratom research and training program 2014-2018 under grant agreement No 633053. The views and opinions expressed herein do not necessarily reflect those of the European Commission.

References

- [1]T. Hirai, F. Escourbiac, S. Carpentier-Chouchana, A. Fedosov, L. Ferrand, T. Jokinen, V. Komarov, A. Kukushkin, M. Merola, R. Mitteau, R. Pitts, W. Shu, M. Sugihara, B. Riccardi, S. Suzuki, R. Villari, ITER tungsten divertor design development and qualification program, Fusion Eng. Des. 88 (2013) 1798 – 1801.
- [2]T. Hirai, F. Escourbiac, S. Carpentier-Chouchana, A. Durocher, A. Fedosov, L. Ferrand, T. Jokinen, V. Komarov, Merola, R. Mitteau, R. A. Pitts, W. Shu, M. Sugihara, V. Barabash, V. Kuznetsov, B. Riccardi, S. Suzuki, ITER full tungsten divertor qualification program and

- progress, *Phys. Scrip.* 2014 (T159) (2014) 014006.
- [3] G. Pintsuk, I. Bobin-Vastra, S. Constans, P. Gavila, M. Rödiger, B. Riccardi, Qualification and post-mortem characterization of tungsten mock-ups exposed to cyclic high heat flux loading, *Fusion Eng. Des.* 88 (2013) 1858 – 1861.
- [4] G. Pintsuk, M. Bednarek, P. Gavila, S. Gerzoskovitz, J. Linke, P. Lorenzetto, B. Riccardi, F. Escourbiac, Characterization of ITER tungsten qualification mock-ups exposed to high cyclic thermal loads, *Fusion Eng. Des.* <http://dx.doi.org/10.1016/j.fusengdes.2015.01.037>.
- [5] Y. Ishijima, H. Kurishita, K. Yubuta, H. Arakawa, M. Hasegawa, Y. Hiraoka, T. Takida, K. Takebe, Current status of ductile tungsten alloy development by mechanical alloying, *J. Nucl. Mater.* 775 (2004) 329–333.
- [6] M. Li, E. Werner, J.-H. You, Fracture mechanical analysis of tungsten armor failure of a water-cooled divertor target, *Fusion Eng. Des.* 89 (2014) 2716 – 2725.
- [7] J. Lemaitre, J.-L. Chaboche, *Mechanics of Solid Materials*, 1st Ed., Cambridge University Press, 1994.
- [8] P. J. Armstrong, C. Frederick, A mathematical representation of the multiaxial Bauschinger effect, G.E.G.B. Report RD/B/N (1966) 731.
- [9] J. Chaboche, Constitutive equations for cyclic plasticity and cyclic viscoplasticity, *Int. J. Plasticity* 5 (1989) 247–302.
- [10] J.-H. You, M. Miskiewicz, Material parameters of copper and CuCrZr alloy for cyclic plasticity at elevated temperatures, *J. Nucl. Mater.* 373 (2008) 269–274.
- [11] ITER structural design criteria for in-vessel components (SDC-IC) Appendix A: Materials design limit data, ITER, (2001).
- [12] ITER Material Properties Handbook, ITER Document No.G74 MA 16, 2005.
- [13] E. N. Sieder, G. E. Tate, Heat transfer and pressure drop of liquids in tubes, *Indust. Eng. Chem.* 28 (1936) 1429–1435.
- [14] J. Thom, W. Walker, T. Fallon, G. Reising, Boiling in sub-cooled water during flow up heated tubes or annuli., *Proc. Inst. Mech. Engineers (London)*, 180: Pt 3C, 226-46(1965-66).
- [15] PLANSEE, Tungsten material properties & applications, www.plansee.com/en/Materials-Tungsten-403.htm.
- [16] M. Li, E. Werner, J.-H. You, Low cycle fatigue behavior of ITER-like divertor target under DEMO-relevant operation conditions, *Fusion Eng. Des.* 90 (2015) 88 – 96.

- [17] M. Li, E. Werner, J.-H. You, Cracking behavior of tungsten armor under ELM-like thermal shock loads: A computational study, *Nucl. Mater. Energy* 2 (2015) 1 – 11.
- [18] B. Gludovatz, S. Wurster, A. Hoffmann, R. Pippan, Fracture toughness of polycrystalline tungsten alloys, *Int. J. Refract. Metals Hard Mater.* 28 (2010) 674–678.

Figure captions

Fig. 1. Metallographic cross section of a prototypical ITER divertor target component after HHF test at 20 MW/m^2 (300 HHF load cycles) [3].

Fig. 2. Geometry and mesh of the FEA model (symmetric quarter part model).

Fig. 3. Schematic illustration of the thermal history considered for modelling.

Fig. 4. Temperature field in the divertor target under stationary HHF load of 20 MW/m^2 .

Fig. 5. Accumulated equivalent plastic strain field in the tungsten armor block after the 5th HHF load cycle at 20 MW/m^2 . Only the tungsten armor block is shown.

Fig. 6. Accumulated equivalent plastic strain at the reference node as a function of time for different HHF loads.

Fig. 7. Experimental LCF data of two different tungsten grades (stress-relieved and annealed) fitted by the Manson Coffin relation [12].

Fig. 8. Evolution of surface temperature and the maximum accumulated equivalent plastic strain over the common time scale of HHF pulse at 20 MW/m^2 (5th HHF load cycle).

Fig. 9. Thermal stress fields (normal component x direction) in the tungsten armor block at 5th HHF load cycle at 20 MW/m^2 during heating (left) and during cooling (right). The tube and the interlayer are not shown.

Fig. 10. Locations of crack considered for the fracture mechanics analysis. The length of the pre-cracks was assumed to be 0.5 mm long.

Fig. 11. J -integral values of the surface crack (crack 1) plotted as a function of crack length. The applied HHF load is 20 MW/m^2 . The recrystallized depth is 4 mm. Two different sets of J -integral values are presented, each calculated either at the free surface edge or at 1st plane of symmetry, respectively. For comparison, the fracture energy (critical J -integral) of stress-relieved tungsten at 400°C is plotted (dotted line).

Fig. 12. J -integral values of crack 2 as a function of crack length. The applied HHF load is 20 MW/m^2 . The recrystallized depth is 4 mm. The fracture energy value (critical J -integral) of stress-relieved tungsten at 400°C is plotted (dotted line) for comparison.

Fig. 13. Maximum J -integral values calculated for the two cracks (crack 1 and crack 2) with a length of 1 mm as a function of HHF loads. The cracks were assumed to locate at the 1st plane

of symmetry.

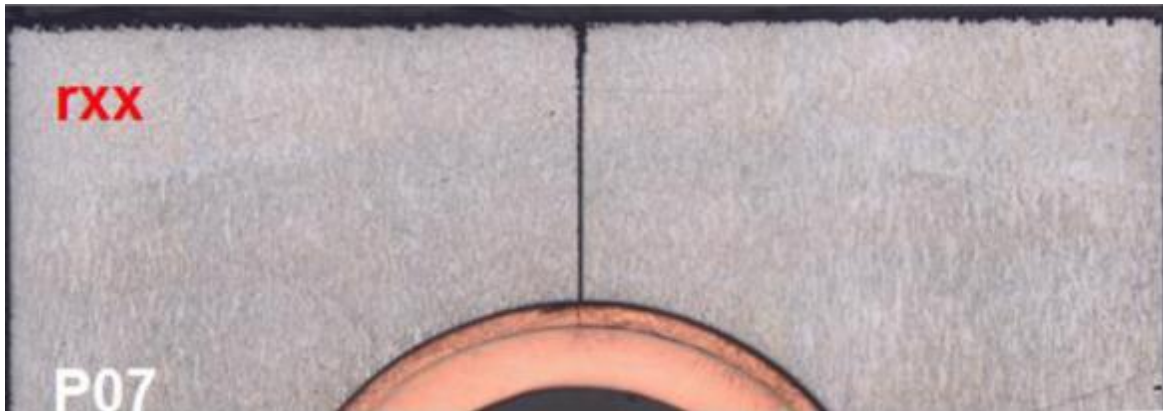


Fig. 1. Metallographic cross section of a prototypical ITER divertor target component after HHF test at 20 MW/m² (300 HHF load cycles) [3].

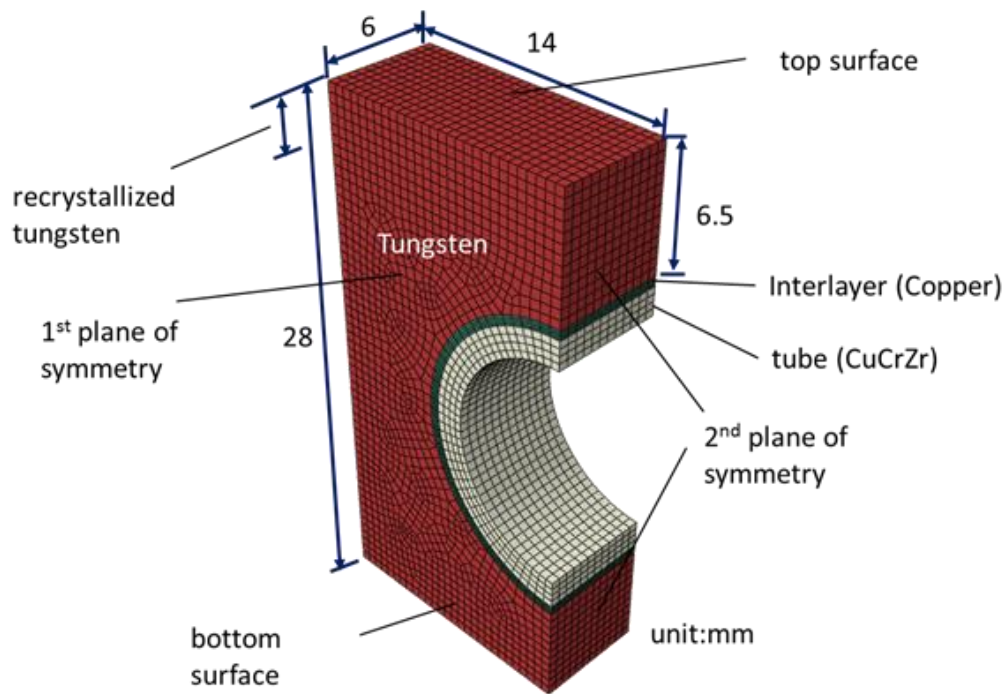


Fig. 2. Geometry and mesh of the FEA model (symmetric quarter part model).

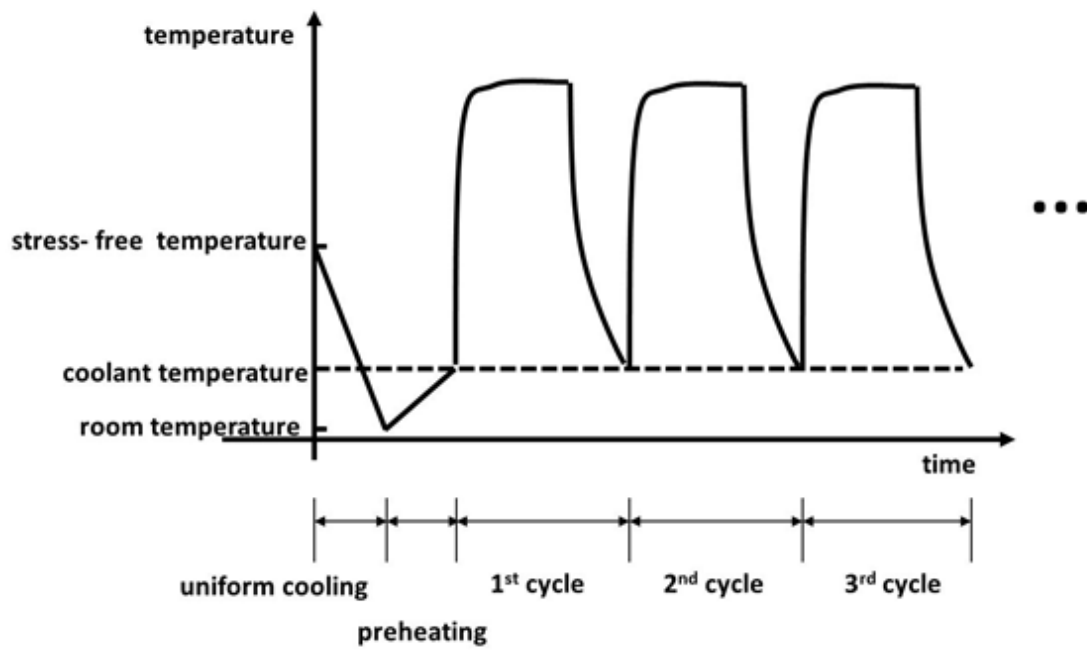


Fig. 3. Schematic illustration of the thermal history considered for modelling.

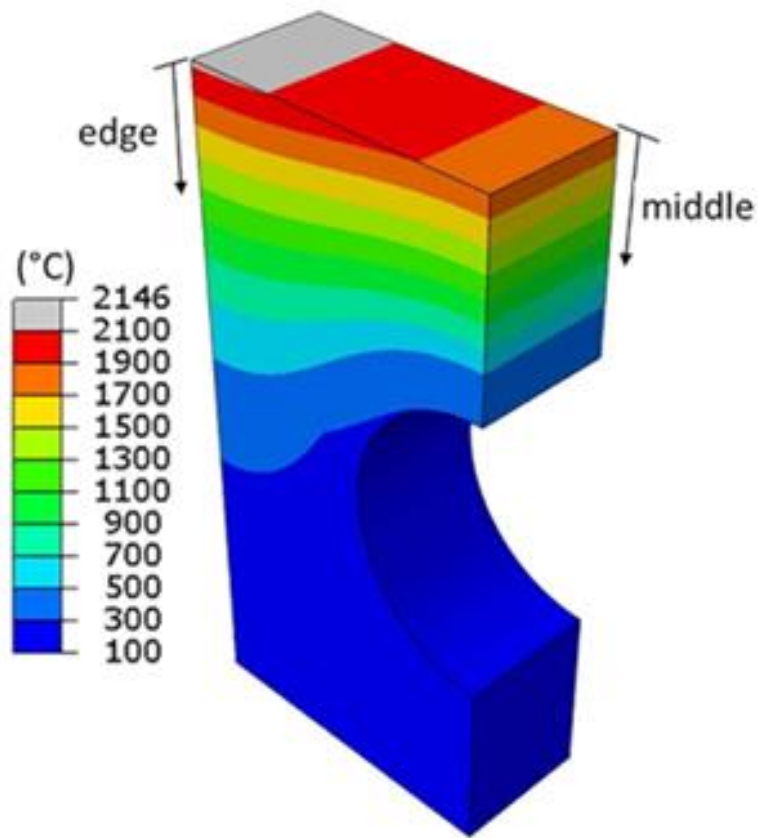


Fig. 4. Temperature field in the divertor target under stationary HHF load of 20 MW/m².

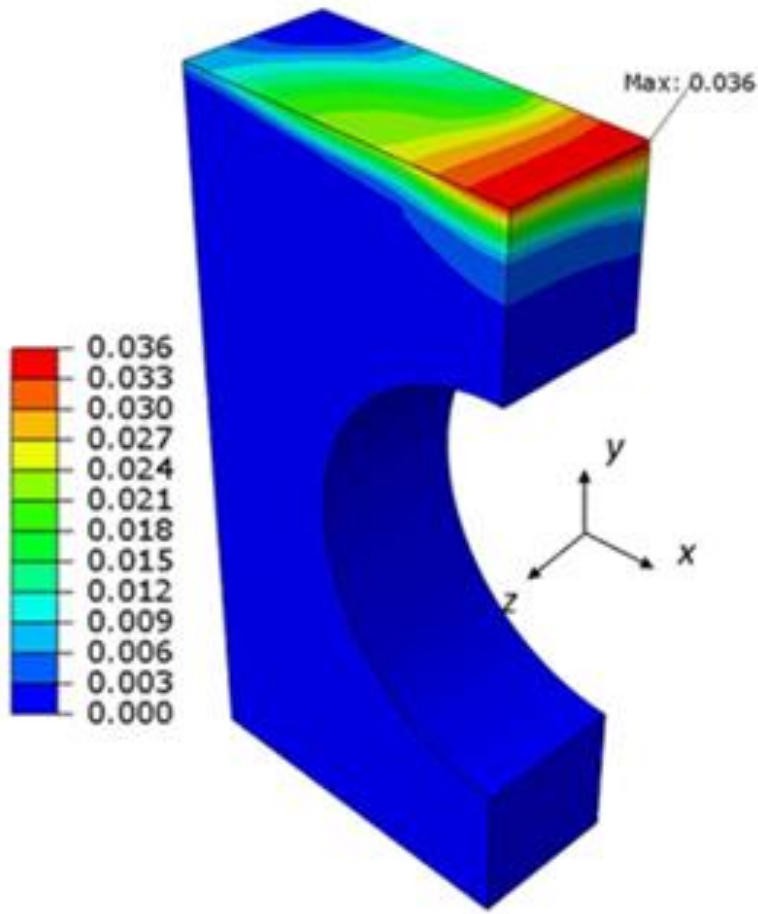


Fig. 5. Accumulated equivalent plastic strain field in the tungsten armor block after the 5th HHF load cycle at 20 MW/m². Only the tungsten armor block is shown.

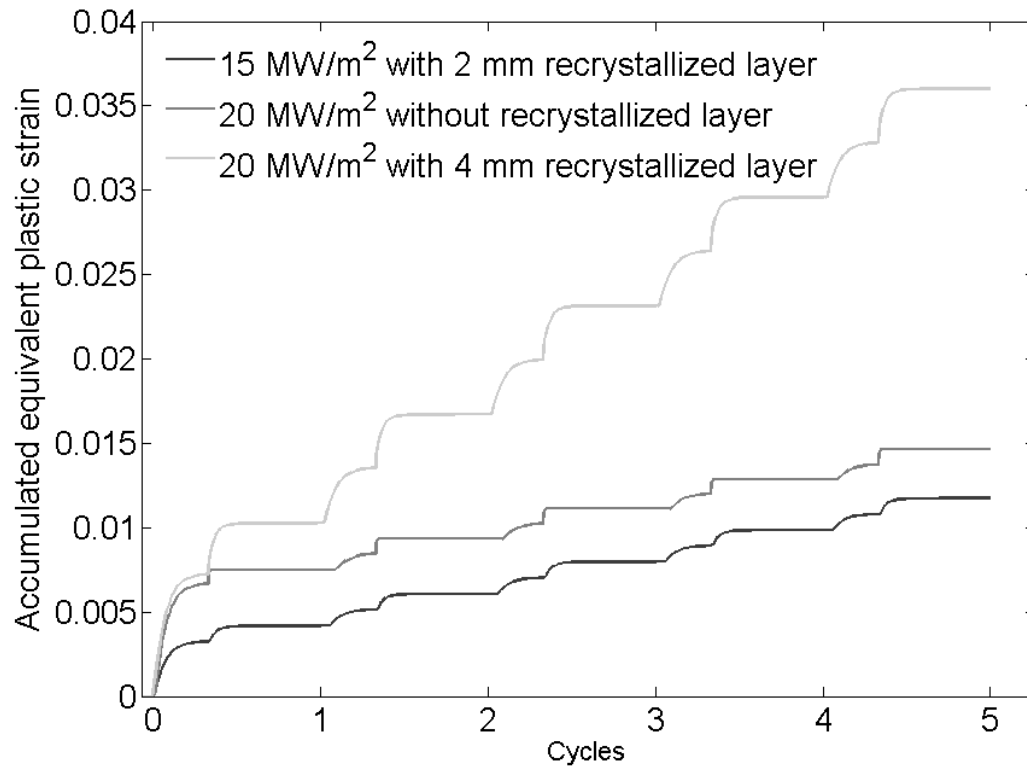


Fig. 6. Accumulated equivalent plastic strain at the reference node as a function of time for different HHF loads.

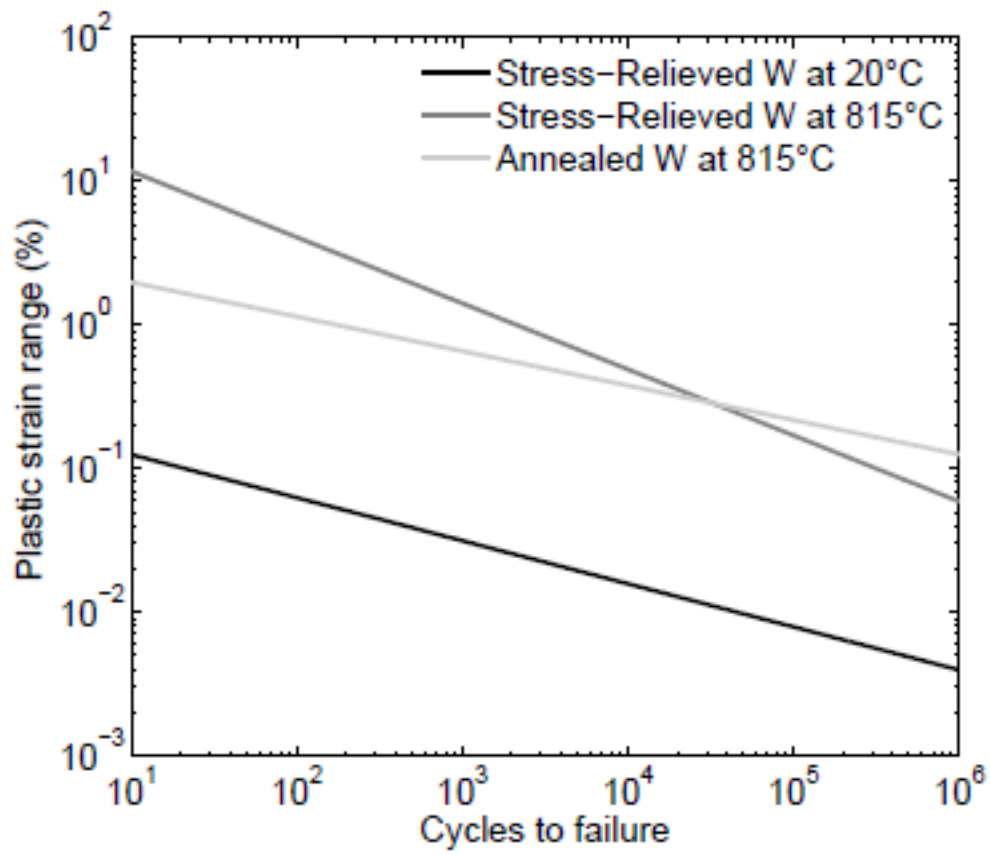


Fig. 7. Experimental LCF data of two different tungsten grades (stress-relieved and annealed) fitted by the Manson Coffin relation [12].

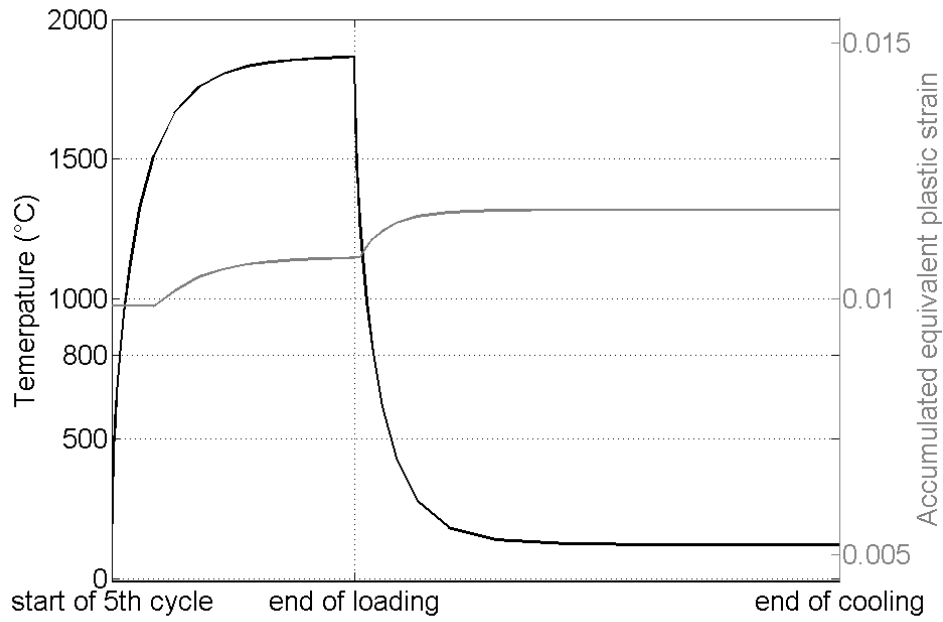


Fig. 8. Evolution of surface temperature and the maximum accumulated equivalent plastic strain over the common time scale of HHF pulse at 20 MW/m² (5th HHF load cycle).

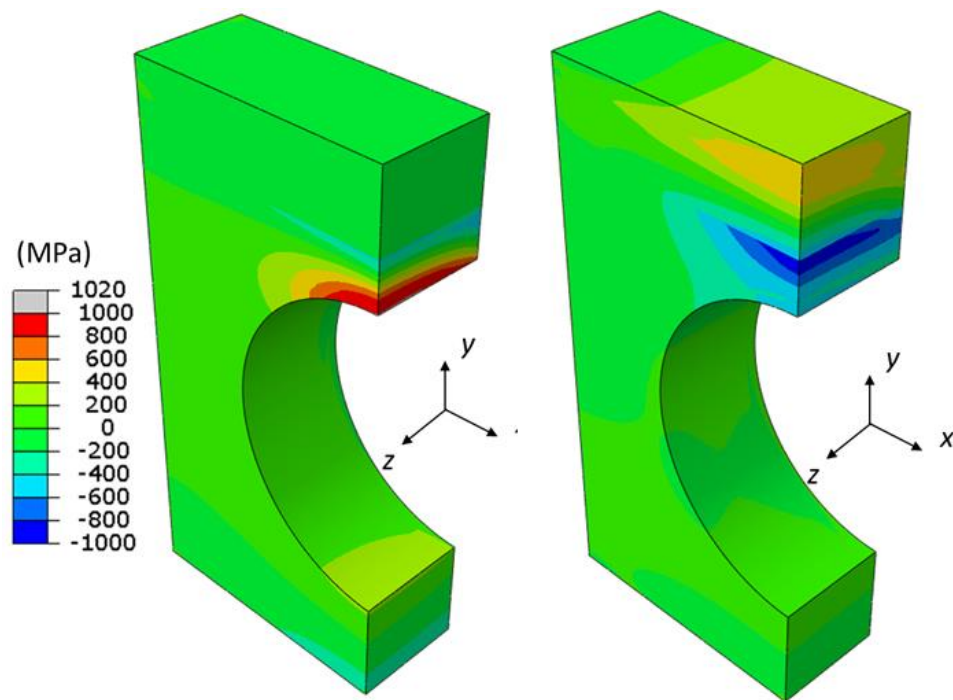


Fig. 9. Thermal stress fields (normal component x direction) in the tungsten armor block at 5th HHF load cycle at 20 MW/m² during heating (left) and during cooling (right). The tube and the interlayer are not shown.

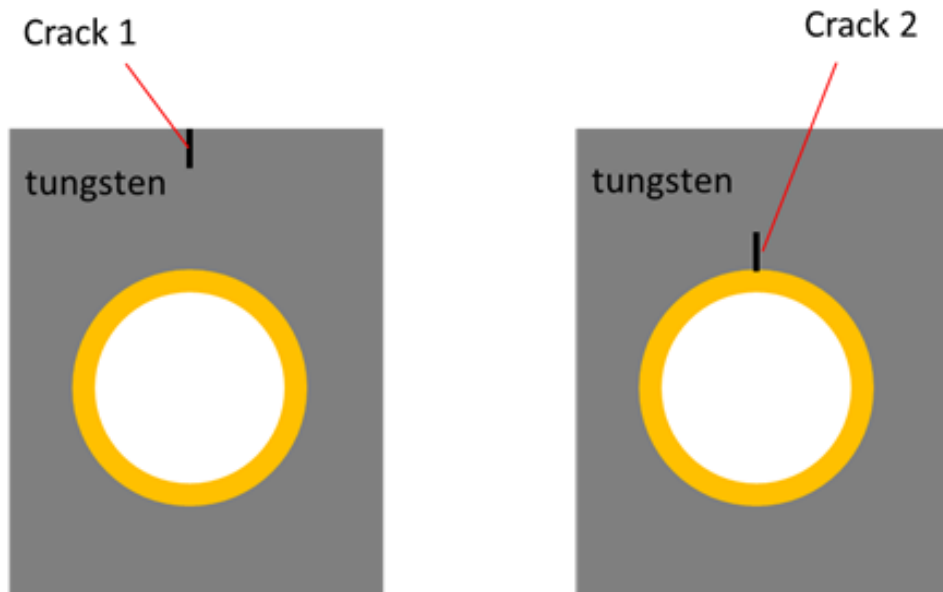
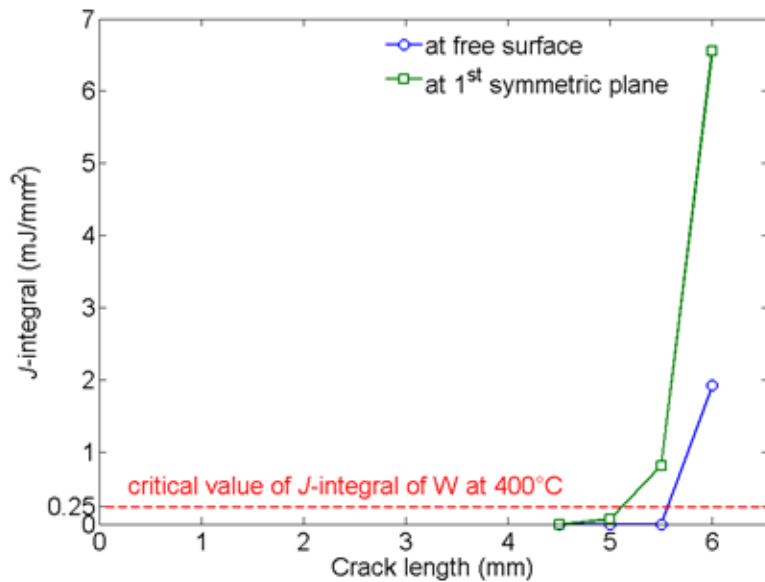
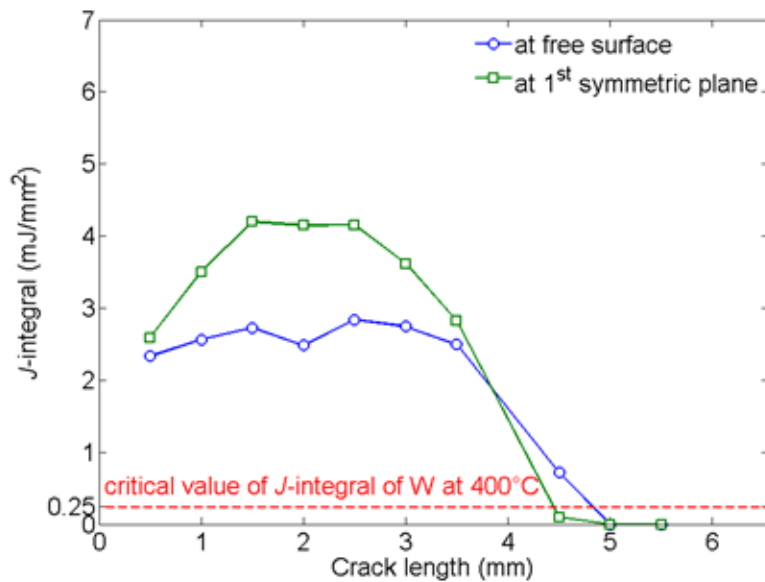


Fig. 10. Locations of crack considered for the fracture mechanics analysis. The length of the pre-cracks was assumed to be 0.5 mm long.



(a) Calculated at end of heating



(b) Calculated at end of cooling

Fig. 11. J-integral values of the surface crack (crack 1) plotted as a function of crack length. The applied HHF load is 20 MW/m². The recrystallized depth is 4 mm. Two different sets of J-integral values are presented, each calculated either at the free surface edge or at 1st plane of symmetry, respectively. For comparison, the fracture energy (critical J-integral) of stress-relieved tungsten at 400 °C is plotted (dotted line).

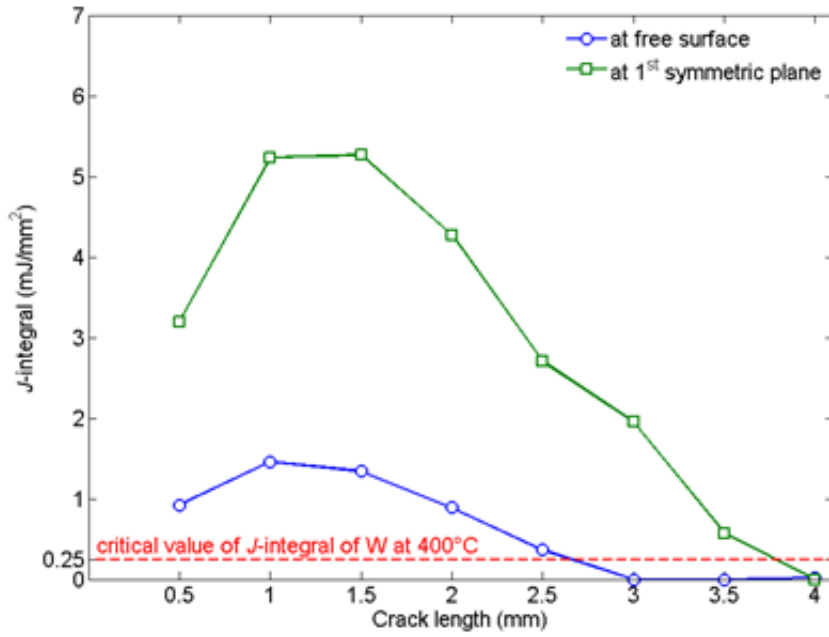


Fig. 12. J-integral values of crack 2 as a function of crack length. The applied HHF load is 20 MW/m². The recrystallized depth is 4 mm. The fracture energy value (critical J-integral) of stress-relieved tungsten at 400 °C is plotted (dotted line) for comparison.

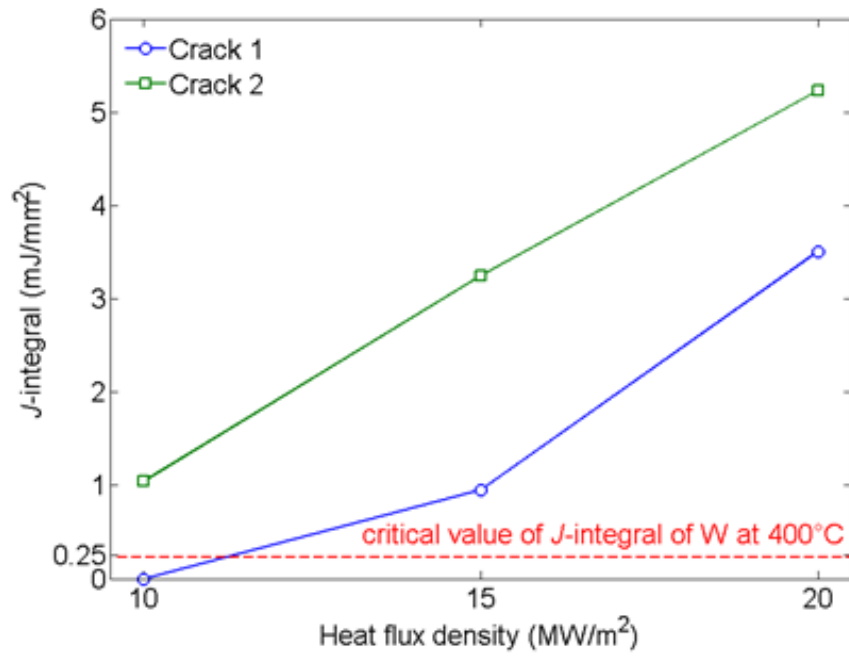


Fig. 13. Maximum J-integral values calculated for the two cracks (crack 1 and crack 2) with a length of 1 mm as a function of HHF loads. The cracks were assumed to locate at the 1st plane of symmetry.